Comparison of Lateral Controllers for Autonomous Vehicles Based on Passenger Comfort Optimization

Akos Mark Bokor[1] [a], Adam Szabo[2] [b], Szilard Aradi[2] [c] and Laszlo Palkovics[1,3] [d]

[1]*Systems and Control Laboratory, HUN-REN Institute for Computer Science and Control (SZTAKI),
Kende utca 13-17., H-1111 Budapest, Hungary*
[2]*Department of Control for Transportation and Vehicle Systems, Faculty of Transportation Engineering and Vehicle
Engineering, Budapest University of Technology and Economics, Műegyetem rkp. 3., H-1111 Budapest, Hungary*
[3]*Széchenyi István University, Egyetem tér 1., H-9026 Győr, Hungary*

Keywords: Autonomous Vehicles, Genetic Algorithm, Model-Based Control, Optimization.

Abstract: This paper focuses on the design of lateral controllers for autonomous vehicles. To enhance passenger comfort while concurrently maintaining minimal deviation from the desired trajectory, the developed controllers are tuned by a Genetic Algorithm, whose cost function is following the ISO 2631 Standard. Three model-based controllers, a Linear Quadratic Regulator, a Linear Quadratic Servo algorithm, and a Model Predictive Controller have been compared in a simulation environment. The test case consists of a suburban road section, where the vehicles must successfully traverse at different velocities while minimizing the lateral acceleration and jerk affecting the passengers. To take into account the velocity-dependent dynamics of the system, the controllers are based on a Linear Parameter-Varying model of the system. The results show that the developed controllers meet the specified requirements regarding the equivalent acceleration, Motion Sickness Dose Value, and deviation from the desired trajectory.

1 INTRODUCTION

Research into vehicle lateral control has been an ongoing endeavor since the 1950s and remains a critical aspect of autonomous vehicle design in the face of evolving technological needs and challenges. Algorithms based on geometric principles such as Pure Pursuit (Samuel et al., 2016) and Stanley controllers (AbdElmoniem et al., 2020) have been successfully used in several cases. Yet, these controllers often fail at handling more complex, dynamic driving tasks. Subsequently, model-based solutions were introduced. Initially, these were based on linear models, but they have progressively shifted towards more complex nonlinear model-based strategies (Menhour et al., 2012). Each evolution offers distinct advantages and confronts specific limitations, particularly the challenge of dealing with variable system parameters that complicate the development of fixed-gain controllers.

[a] https://orcid.org/0009-0005-4845-9923
[b] https://orcid.org/0000-0003-1633-5588
[c] https://orcid.org/0000-0001-6811-2584
[d] https://orcid.org/0000-0001-5872-7008

Over the years, several key considerations have shaped the design of lateral controllers. These include robust stability, computational capacity, and precise reference signal tracking (Gáspár et al., 2016; Tagne et al., 2015). However, integrating passenger comfort into control system designs has become essential as the industry achieves SAE Level 5 autonomy. This integration is crucial for enhancing marketability and providing a human-like driving experience (Cascetta et al., 2022). In recent years, this goal has been pursued through machine learning algorithms. For example, (Zhang et al., 2018) presents an approach that utilizes a deep reinforcement learning algorithm to replicate human-like car-following behavior with higher accuracy and adaptability than traditional models. This integration ensures a more accurate imitation of human driving styles and continuously updates the models with new data, enhancing the system's adaptability and reliability in diverse driving scenarios (Zhu et al., 2018), which is essential for guaranteeing user safety and building trust in autonomous systems. This can be achieved through various approaches; for instance, (Poussot-Vassal et al., 2011) emphasizes using gain scheduling techniques

to adjust control parameters, enhancing vehicle dynamic stability.

The method proposed in (Li et al., 2019) breaks the vision-based lateral control system down into a perception and a control module. While the algorithm outperformed model-based algorithms, there are no guarantees regarding their robustness and stability. Hence, another approach is to combine machine-learning-based solutions with more conventional control systems. Such an example is presented in (Mashadi et al., 2014), where a Genetic Algorithm is utilized to optimize a PID controller.

Besides ensuring precise reference tracking, the emphasis on optimizing passenger comfort is rapidly increasing. However, improved precision comes at the cost of higher lateral acceleration, which may negatively impact passenger comfort.(Tagne et al., 2015; Mesghali, 2021) Addressing the trade-off between precision in tracking and passenger comfort is particularly acute at higher speeds, where sharper maneuvers lead to greater lateral accelerations. To mitigate these effects, implementing a speed-dependent controller design is crucial. Techniques such as Gain Scheduling and Linear Parameter Varying (LPV) control offer viable solutions to adjust controller gains based on vehicle speed (Németh and Gáspár, 2011; Zin et al., 2008; Tóth, 2010), thus optimizing both performance and comfort across varying driving conditions.

1.1 Related Work

Numerous methodologies exist for the design of controllers that prioritize passenger comfort as a fundamental criterion for optimization. One such technique involves minimizing the Motion Sickness Dose Value (MSDV). The MSDV, adhering to the ISO 2631-1 standards, provides a quantitative index of passenger comfort by explicitly accounting for the effects of motion on the human vestibular system. The algorithm proposed in (Moreno-Gonzalez et al., 2022) is engineered to mitigate motion-induced discomfort among passengers by adeptly managing vehicle dynamics, including acceleration and jerk.

In addition to minimizing the MSDV, passenger comfort considerations can also be integrated into the controller design. In (Sever et al., 2021), a gain-scheduled Linear Quadratic Regulator (LQR) controller is employed for this purpose, incorporating modifications to account for both vertical and horizontal motion components. This consideration is critical, as passengers, no longer needing to focus on driving, may engage in activities that heighten their susceptibility to motion sickness. A more traditional

approach is presented in (Luciani et al., 2020), where the controllers are tuned concerning vehicle dynamics and passenger comfort. The proposed method integrates these considerations through a specialized Model Predictive Control (MPC) design, optimizing standard metrics for vibration and motion sickness within the broader context of vehicle control.

These papers demonstrate that incorporating passenger comfort considerations into controller design does not significantly diminish the controllers' path-following capabilities. Instead, they produce substantially better comfort outcomes than controllers designed solely for path-following. However, there is a notable gap in research comparing these optimized controllers despite the potential for varying results in both simulations and practical applications. This highlights the importance of conducting more comparative analyses to understand their relative effectiveness under similar comfort considerations.

1.2 Contributions

This paper presents three model-based lateral controllers, which are tuned through an optimization algorithm that incorporates a cost function consisting of tracking accuracy and passenger comfort-related requirements. The presented controllers are evaluated and compared based on their performance with respect to the equivalent acceleration, MSDV, and lateral deviation.

The paper is organized as follows: Section 2 presents the Linear Parameter-Varying model describing the lateral vehicle dynamics. Section 3 and Section 4 describe the implemented control algorithms and the applied optimization algorithm. Section 5 deals with the simulation environment and test cases, while Section 6 presents the evaluation of the results. Section 7 shows some concluding remarks.
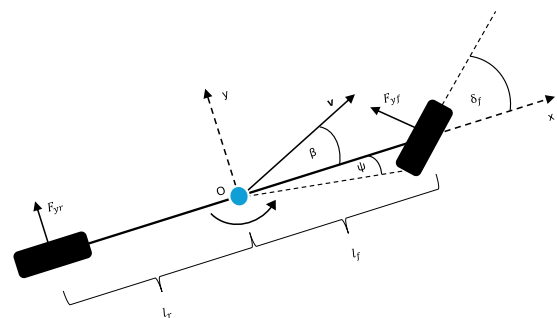

Figure 1: Lateral vehicle dynamics.

2 LATERAL VEHICLE MODEL

This paper uses a modified variant of the widely known dynamic bicycle model, representing the vehicle as a two-wheel-point system. Figure 1 shows the lateral vehicle dynamics.

The equations of motion are derived as follows by applying Newton's second law and neglecting the impact of road bank angle:

$$ma_y = F_{yf} + F_{yr} \qquad (1)$$

where a_y is the inertial acceleration of the vehicle at the center of gravity (c.g.) of the vehicle along the y-axis, m is the mass of the vehicle, and F_{yf} and F_{yr} are the front and rear lateral tire forces, respectively.

The inertial acceleration of the vehicle consists of two components: lateral acceleration and centripetal acceleration. Hence, the lateral motion of the vehicle can be written as follows:

$$m(\ddot{y} + V_x \dot{\psi}) = F_{yf} + F_{yr} \qquad (2)$$

where $\ddot{y}$ is the lateral acceleration of the vehicle, V_x is the longitudinal velocity at the c.g., and $\dot{\psi}$ is the yaw rate.

The torque balance equation, which defines the yaw dynamics of the vehicle, is written as follows:

$$I_z \ddot{\psi} = \ell_f F_{yf} - \ell_r F_{yr} \qquad (3)$$

where I_z is the inertia of the vehicle along the z-axis, ℓ_f and ℓ_r are the distances between the c.g. of the vehicle and the front and rear tires, respectively.

Accounting for the interdependence between tire forces and steering dynamics, the lateral tire forces F_{yf} and F_{yr} are calculated by determining the relationship between slip angle and lateral force. The slip angle, which is the difference between the orientation of the wheel and the wheel velocity vector, directly influences the lateral forces.

Assuming a linear relationship between the tire forces and the slip, the front and rear lateral tire forces are defined as follows:

$$F_{yf} = 2C_f(\delta - \theta_{yf}) \qquad (4)$$

$$F_{yr} = 2C_r(-\theta_{yr}) \qquad (5)$$

where C_f and C_r represent the cornering stiffness coefficients of the front and rear tires, δ is the steering angle, while θ_{yf} and θ_{yr} denote the angles of the front and rear wheel velocity vectors, which are approximated using the small-angle assumptions:

$$\theta_{yf} = \frac{\dot{y} + \ell_f \dot{\psi}}{V_x} \qquad (6)$$

$$\theta_{yr} = \frac{\dot{y} - \ell_r \dot{\psi}}{V_x} \qquad (7)$$

The conventional bicycle model can be formulated using Equations (1-7). However, based on (Rajamani, 2011), redefining the state variables to represent the position and orientation error of the vehicle with respect to the desired trajectory yields a more suitable form for the development of a steering control system. The state vector of the modified model is the following:

$$x = \begin{bmatrix} e_1 & \dot{e}_1 & e_2 & \dot{e}_2 \end{bmatrix}^T \qquad (8)$$

where e_1 represents the lateral deviation of the vehicle from the road centerline, and e_2 represents the orientation error relative to the road direction.

To follow the defined trajectory, the desired yaw rate of the vehicle shall be calculated as follows:

$$\dot{\psi}_{des} = V_x \kappa \qquad (9)$$

where κ is the road curvature at the selected reference point.

Through the desired yaw rate and assuming constant longitudinal velocity, the derivatives of the error states are defined as follows:

$$\ddot{e}_1 = \ddot{y} + V_x(\dot{\psi} - \dot{\psi}_{des}) \qquad (10)$$

$$\dot{e}_1 = \dot{y} + V_x(\psi - \psi_{des}) \qquad (11)$$

$$e_2 = \psi - \psi_{des} \qquad (12)$$

$$\dot{e}_2 = \dot{\psi} - \dot{\psi}_{des} \qquad (13)$$

Assuming $\ddot{\psi}_{des}$ to be equal to zero, and combining Equations (1-13) into Equation (14), the model can be written in state-space representation.

From a control design point of view, the system has a controllable input δ and an uncontrollable input $\dot{\psi}_{des}$, which is neglected during the synthesis of the feedback controllers.

The resulting state and input matrices depend on the longitudinal velocity of the vehicle; thus, the system shows time-varying properties. Therefore, the model is formulated using a grid-based LPV representation. While a wide variety of LPV-based control approaches are available to handle such systems, the longitudinal velocity of the vehicle varies slowly in most applications. Hence, the presented algorithms use gain scheduling to deal with the time-varying nature of the system.

3 CONTROL SYNTHESIS

This section details the theoretical background and implementation of the presented controllers, including a Linear Quadratic Regulator (LQR), a Linear

$$\frac{d}{dt}\begin{bmatrix} e_1 \\ \dot{e}_1 \\ e_2 \\ \dot{e}_2 \end{bmatrix} = \begin{bmatrix} 0 & 1 & 0 & 0 \\ 0 & -\frac{2C_f+2C_r}{mV_x} & \frac{2C_f+2C_r}{mV_x} & \frac{-2C_fl_f+2C_rl_r}{mV_x} \\ 0 & 0 & 0 & 1 \\ 0 & -\frac{2C_fl_f-2C_rl_r}{I_zV_x} & \frac{2C_fl_f-2C_rl_r}{I_z} & -\frac{2C_fl_f^2+2C_rl_r^2}{I_zV_x} \end{bmatrix}\begin{bmatrix} e_1 \\ \dot{e}_1 \\ e_2 \\ \dot{e}_2 \end{bmatrix} + \begin{bmatrix} 0 \\ \frac{2C_f}{m} \\ 0 \\ \frac{2C_fl_f}{I_z} \end{bmatrix}\delta + \begin{bmatrix} 0 \\ -\frac{2C_fl_f+2C_rl_r}{mV_x} - V_x \\ 0 \\ -\frac{2C_fl_f^2+2C_rl_r^2}{I_zV_x} \end{bmatrix}\dot{\psi}_{des} \quad (14)$$

Quadratic Servo (LQ-Servo), and a Model Predictive Controller (MPC). The controllers presented in this paper have been implemented in discrete time with $1ms$ sampling time.

3.1 Linear Quadratic Regulator

The Linear Quadratic control problem is fundamental in control theory (Athans and Falb, 2013). The first step of the LQR synthesis is to transform the model presented in Equation (14) into a discrete-time state-space model:

$$x(k+1) = Ax(k) + Bu(k) \quad (15)$$
$$y(k) = Cx(k) + Du(k) \quad (16)$$

where $x(k)$ is the state vector at time step k, $u(k)$ is the input vector, A is the state transition matrix, and B is the input matrix. $y(k)$ is the output vector, C is the output matrix, and D is the feedthrough matrix.

Therefore, (ψ_{des}), the uncontrollable input of the model is neglected, and then the presented continuous model is discretized with $1ms$ sample time.

The objective of the LQR controller is to minimize a quadratic cost function that considers the weighted sum of the state and input vectors over an infinite horizon:

$$J = \sum_{k=0}^{\infty}(x(k)^TQx(k) + u(k)^TRu(k)) \quad (17)$$

where Q and R are positive (semi-)definite matrices that weight the state and input vectors, respectively. The minimum of the cost function can be found by solving the Discrete-time Algebraic Riccati Equation (DARE):

$$A^TPA - P - A^TPB(B^TPB+R)^{-1}B^TPA + Q = 0 \quad (18)$$

where P is a positive definite matrix, the solution of the Riccati Equation. Using P, the optimal feedback gain K is then determined as:

$$K = (B^TPB+R)^{-1}B^TPA \quad (19)$$

The optimal control input minimizing the cost function is given as:

$$u(k) = -Kx(k) \quad (20)$$

3.2 Linear Quadratic Servo

The linear quadratic servo approach augments the output of the system with an integrator to ensure zero steady-state error and achieve more accurate trajectory tracking:

$$\begin{bmatrix} x(k+1) \\ z(k+1) \end{bmatrix} = \begin{bmatrix} A & 0 \\ -C & 0 \end{bmatrix}\begin{bmatrix} x(k) \\ z(k) \end{bmatrix} + \begin{bmatrix} B \\ I \end{bmatrix}u(k) \quad (21)$$

where I is an identity matrix, and $z(k)$ is the integral of the output error.

Solving the Riccati equation for the augmented system gives the following feedback gain:

$$K_I = \begin{bmatrix} K \\ K_z \end{bmatrix} = -(R+B^TPB)^{-1}(B^TPA) \quad (22)$$

Then, the optimal control input for LQ-Servo is written as:

$$u(k) = -Kx(k) - K_zz(k) \quad (23)$$

3.3 Model Predictive Control

At last, an MPC has been implemented based on (Wang, 2009), which solves a finite horizon, constrained optimization problem.

To ensure integral action, the state-space model is reformulated in terms of state changes:

$$\Delta x(k) = x(k) - x(k-1) \quad (24)$$
$$\Delta u(k) = u(k) - u(k-1). \quad (25)$$

Incorporating these changes into the state equation results in:

$$\Delta x(k+1) = A\Delta x_m(k) + B\Delta u(k). \quad (26)$$

Then, a new state vector is formulated, which connects the state changes and output:

Thus, the augmented state-space model is written as:

$$\hat{x}(k) = \begin{bmatrix} \Delta x(k+1) \\ y(k+1) \end{bmatrix} =$$
$$= \begin{bmatrix} A & 0 \\ CA & 1 \end{bmatrix}\begin{bmatrix} \Delta x(k) \\ y(k) \end{bmatrix} + \begin{bmatrix} B \\ CB \end{bmatrix}\Delta u(k), \quad (27)$$
$$\hat{y}(k) = \begin{bmatrix} 0 & 1 \end{bmatrix}\begin{bmatrix} \Delta x(k) \\ y(k) \end{bmatrix} \quad (28)$$

were 0 is a zero vector matching the state vector x in size, and ˆ denotes the elements of the augmented state-space model.

The augmented state-space equations are following:

$$\hat{x}(k+1) = \hat{A}x(k) + \hat{B}\Delta u(k), \qquad (29)$$

$$\hat{y}(k) = \hat{C}\hat{x}(k). \qquad (30)$$

The MPC algorithm aims to solve the following constrained optimization problem:

$$\min_{\Delta U} \quad J(\Delta U) = \sum_{k=1}^{N_p} y_i^T Q y_i + \sum_{k=1}^{N_c} \Delta u_i^T R \Delta u_i \qquad (31)$$

$$s.t.$$

$$\Delta u_{min} \leq \Delta u(k) \leq \Delta u_{max} \qquad \forall k \in N_c$$

$$u_{min} \leq u(k) \leq u_{max} \qquad \forall k \in N_c$$

where N_p is the prediction horizon, N_c is the control horizon, and Δu_{min}, Δu_{max}, u_{min}, u_{max} are the constraints on the gradient and magnitude of the input signal.

The presented constrained optimization problem is typically solved using quadratic programming (QP), as it is an effective way to sort out the active constraints. On the other hand, utilizing the receding horizon control principle of MPC, it is possible to impose the constraints only on the first samples of the variables.
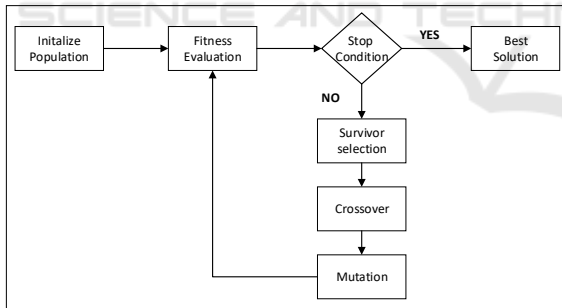

Figure 2: Blockdiagram of the Genetic Algorithm.

4 OPTIMIZATION

Given that the designed controllers are configured as Single-Input Single-Output (SISO) systems, tuning the R parameter in the cost function to adhere to the specified passenger comfort criteria is sufficient. This tuning approach accelerates the optimization process and reduces computational demands. To find the controller parameters, the Genetic Algorithm (GA) optimization method (Mathew, 2012) has been selected. Its simplified process is depicted in Figure 2.

The core of the GA starts with the initialization of a population, which in this paper consisted of 20 individuals. Each individual, represented as a chromosome, encodes a potential solution to the optimization problem. The diversity within this initial population is crucial as it affects the ability of the algorithm to explore different areas of the solution space effectively.

The fitness of each chromosome is assessed based on its suitability to solve the problem at hand, which, in this case, was guided by a fitness function defined as follows:

$$J_{total} = J_{a_y} + J_{\dot{a}_y} + J_{e_1} + J_\delta \qquad (32)$$

where J_{a_y}, $J_{\dot{a}_y}$, J_{e_1} and J_δ are the penalty on lateral acceleration, lateral jerk, lateral deviation, and steering angle, respectively.

Each term of the fitness function is calculated using the same equation, which is provided for the lateral acceleration term as an example:

$$J_{a_y} = \begin{cases} \frac{\int_{t=0}^{T}(a_{y,max}-|a_y|)^2}{T} W_{a_y} & if\ |a_y| > a_{y,max} \\ 0 & otherwise \end{cases} \qquad (33)$$

where W_{a_y} is a weight derived from Bryson's rule, T is the simulation time, and $a_{y,max}$ is the maximum allowed acceleration. The maximum allowed values have been determined based on the ISO 2631 standard, the desired tracking accuracy, and the physical limitations of the steering actuator.

The objective is to minimize oscillations, maximize the smoothness of the control process, reduce lateral deviations from the desired path, and control the peaks in the steering angles. This comprehensive approach ensures that the optimization enhances comfort by smoothing acceleration and jerk and improves path tracking and steering behavior.

After evaluating the fitness of the population, the algorithm checks if the stopping condition is met. This study defined the stopping condition as reaching a maximum of 60 generations. If the stopping condition is not met, the algorithm proceeds with the selection of individuals for the next generation. This selection is typically based on fitness values, where better-performing individuals are more likely to be selected, ensuring that the advantageous traits are carried forward.

The selected individuals then undergo crossover and mutation processes. Crossover involves combining pairs of individuals (parents) to produce new individuals (offspring) by exchanging segments of their chromosomes, thereby creating diversity while preserving useful genetic information. Mutation introduces random changes to individual chromosomes, which helps maintain genetic diversity within the

population and prevents premature convergence to suboptimal solutions. Each iteration of this process determines a new R value based on the current population. This value is then used to re-evaluate the fitness function in the next iteration. This iterative process continues until the fitness function converges to an optimal solution, ensuring that the GA effectively tunes the R parameter to meet the specified passenger comfort criteria.

5 SIMULATION ENVIRONMENT

The control algorithms and optimization processes have been implemented in the Matlab/Simulink environment. The simulation environment has been created in the CarMaker software package. It has been chosen for its ability to simulate real-world conditions accurately and its well-defined Matlab interface.

Table 1: Vehicle Parameters.

Parameter	Symbol	Value	Unit
Mass	m	1463	[kg]
Inertia	I_{zz}	1600	[$kg \cdot m^2$]
Distance from CoM to front axle	l_f	1.1	[m]
Distance from CoM to rear axle	l_r	1.58	[m]
Front cornering stiffness	C_{af}	80000	[N/rad]
Rear cornering stiffness	C_{ar}	80000	[N/rad]

For the simulations, the default vehicle model of CarMaker has been used, whose parameters are listed in Table 1. The lateral acceleration and path deviation have been measured using built-in inertial and road sensors. The jerk was computed by differentiating the acceleration and applying a low-pass filter to reduce noise resulting from numerical differentiation.

The test case consists of a suburban road section, which has been designed for a maximum 50 km/h vehicle speed. Figure 3 illustrates the turning radius and trajectory. According to (Kilinc and Baybura, 2012) and (Jagelčák et al., 2022), the ideal road radius ranges between 230 m and 280 m, which corresponds to a lateral acceleration of 1.47 m/s². Consequently, the curvatures of the road correspond to 230 m and 280 m turning radius.

6 RESULTS

Several key metrics have been considered to facilitate a comprehensive comparison. Based on (Luciani et al., 2020) and the ISO 2631 standard, the equivalent acceleration (a_{eq}) and the MSDV value have been selected as metrics of passenger comfort. Based on the
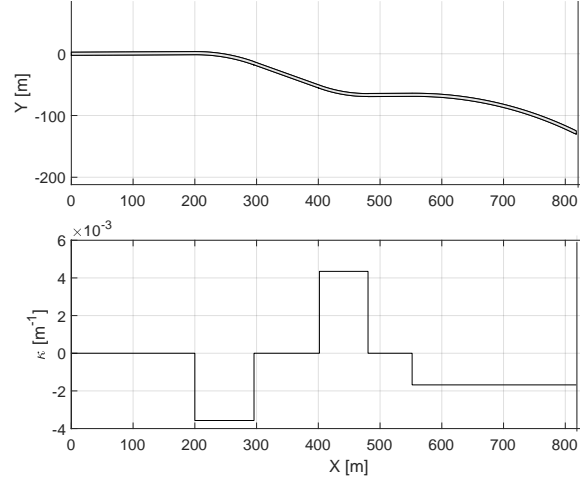

Figure 3: Desired path and road curvature.

likely passenger comfort, the equivalent acceleration has been divided into different categories, shown in Table 2.

Table 2: Likely reactions to various magnitudes of overall vibration total values, specified in ISO 2631-1.

a_{eq} [m/s^2]	Reaction
$a_{eq} \leq 0.315$	Not uncomfortable
$0.315 \leq a_{eq} \leq 0.63$	A little uncomfortable
$0.5 \leq a_{eq} \leq 1$	Fairly uncomfortable
$0.8 \leq a_{eq} \leq 1.6$	Uncomfortable
$1.25 \leq a_{eq} \leq 2.5$	Very uncomfortable
$a_{eq} \geq 2$	Extremely uncomfortable

To determine the equivalent acceleration, first, the frequency-weighted root mean square (WRMS) acceleration along the main axes is calculated as:

$$a_{W_d,\text{RMS}} = \left(\frac{1}{T_f} \int_0^{T_f} a_{W_i}^2(t) \, dt \right)^{\frac{1}{2}} \tag{34}$$

where T_f represents the integration time, a_{W_i} is the frequency-weighted function, and $a_{W_d,\text{RMS}}$ is the root mean square of a_{W_d}.

Then, the equivalent acceleration can be calculated as:

$$a_{eq} = \sqrt{k_x^2 a_{x,W}^2 + k_y^2 a_{y,W}^2} \tag{35}$$

Here, $a_{x,W}$ and $a_{y,W}$ are the frequency-weighted RMS accelerations along the x and y axes, respectively, and k_x and k_y are weighting factors. Assuming $k_x = k_y = 1$ and neglecting the longitudinal acceleration (as the longitudinal acceleration has been constant), a_{eq} can be calculated as the RMS of $a_{y,W}$ over the entire track.

The second index evaluated is the Motion Sickness Dose Value (MSDV), which describes the proba-

bility of motion sickness occurrence due to oscillatory motion. This index is calculated similarly to a_{eq} but uses W_f as the frequency-weighted function. According to the ISO 2631 standard, the likelihood of nausea symptoms is calculated as follows:

$$a_{\mathrm{MSDV}}[\%] = \frac{1}{3} \cdot a_{\mathrm{MSDV}} \times 100 \qquad (36)$$

Furthermore, the performance of the controllers with respect to reference signal tracking and the control input has also been evaluated beyond passenger comfort.
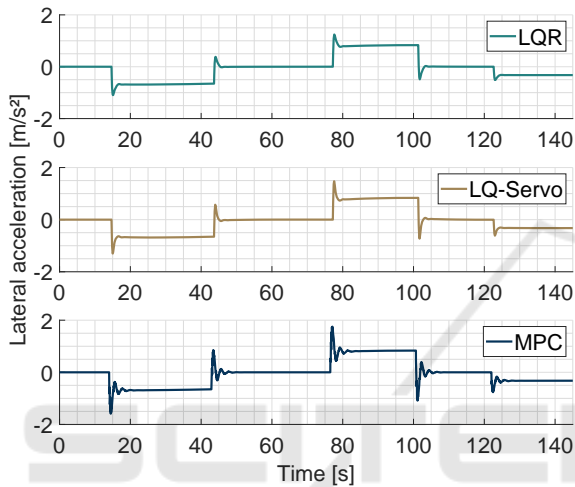

Figure 4: Lateral acceleration of the vehicles at 50 km/h.

As depicted in Figure 4, the observed peaks in acceleration are primarily the result of sudden changes in cornering. These peaks vary significantly among different controllers. In the case of the LQR, the peaks are confined within smaller limits due to the nature of the control strategy. Conversely, the other two controllers show larger acceleration peaks due to their integrating characteristics.

A more detailed examination of the controller performance metrics is presented in Table 3. The data indicates that all three controllers are in the 'not uncomfortable' category with respect to equivalent acceleration (a_{eq}). This observation indicates a relatively uniform level of performance among the controllers concerning passenger comfort across the entire track.

In particular, the LQR and LQ-Servo controllers showed comparable a_{eq} values, underscoring a consistent response to dynamic vehicular motions. In contrast, the Model Predictive Control (MPC) demonstrated slightly elevated a_{eq} values.

Considering the MSDV values, all three controllers achieved approximately 4%, which complies with the regulations.

Regarding the magnitude of the acceleration peaks, the maximum values were most significant in the MPC controller, nearly one and fifty percent greater than those observed with the LQR. This highlights the higher responsiveness of the MPC controller, which is caused by the augmentation of the modified dynamic bicycle model.

The controllers have also been tested on the same track at 70 km/h and 100 km/h speeds. The results of these tests are presented in Table 4. It can be observed that the maximum absolute acceleration and MSDV values increase significantly as the curvature has been defined for a lower maximum speed. However, in terms of equivalent acceleration (a_{eq}), even at 100 km/h, only the MPC controller falls in the middle of the "a little uncomfortable" range, while the other two controllers are near the bottom of this range, almost reaching the "not uncomfortable" category.

Table 3: Controller performance comparison at 50 km/h.

Metric	LQR	LQ-Servo	MPC
a_{eq} [m/s^2]	0.090642	0.096871	0.11723
a_{MSDV} [%]	3.9759	3.9034	4.0441
a_{peak} [m/s^2]	1.193	1.42	1.752
Maximal Jerk [m/s^3]	6.63	10.77	13.96
Average / maximal Lateral Deviation [m]	0.0295 / 0.0731	0.0071 / 0.0594	0.007 / 0.0395
Input signal settling time [s]	0.376	0.426	0.837

While peak accelerations were associated with corresponding increases in jerk magnitudes, higher jerk does not necessarily equate to poorer passenger comfort, according to (de Winkel et al., 2023).
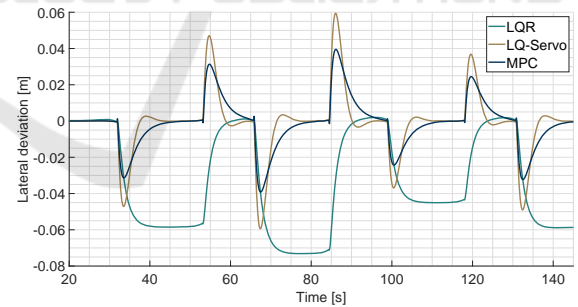

Figure 5: Comparison of the lateral deviations.

As Figure 5 shows, the LQR controller does not reduce the steady-state error due to its lack of an integrating component. In contrast, although it shows larger transient deviations, the LQ-Servo controller effectively reduces this error to zero. This behavior is attributed to the integrating element within the LQ-Servo controller, designed to correct long-term steady-state errors. However, the initial reduction and subsequent overshoot of integrated errors can lead to a delayed response from the controller. The MPC performs best in terms of tracking accuracy. Specifically,

it achieves an order of magnitude smaller maximum lateral deviation over the entire track compared to the LQR controller.

The MPC is tuned to be the most aggressive, resulting in the longest control signal settling time among the controllers.

Table 4: Controller performance comparison at different speeds.

Metric	LQR	LQ-Servo	MPC
50 km/h			
a_{eq} [m/s^2]	0.090642	0.096871	0.11723
a_{MSDV} [%]	3.9759	3.9034	4.0441
Max absolute a_y [m/s^2]	1.2421	1.4737	1.7523
70 km/h			
a_{eq} [m/s^2]	0.18601	0.18636	0.23495
a_{MSDV} [%]	10.5429	10.6457	10.5926
Max absolute a_y [m/s^2]	2.3904	2.427	3.0725
100 km/h			
a_{eq} [m/s^2]	0.35503	0.37098	0.52087
a_{MSDV} [%]	22.9865	23.5348	22.5547
Max absolute a_y [m/s^2]	3.8248	3.9982	5.6173

7 CONCLUSION

This paper compared three model-based controllers in terms of lateral acceleration and jerk as indicators of passenger comfort and reference signal tracking. These properties were optimized using a genetic algorithm to ensure the controllers met the specified criteria. All three controllers complied with the standards described in the relevant regulations.

All three controllers achieved low reference tracking errors while meeting passenger comfort requirements for the given tracking bicycle model and the specified simulation vehicle on the designated track. Considering overall performance, including equivalent acceleration, MSDV, lateral deviation, jerk, and input signal settling time, the LQ-Servo controller proved the most optimal. Although it slightly underperformed compared to the MPC in reference tracking, it demonstrated twice as fast settling times and 20% lower peak accelerations, making it the best choice in this simulation and model structure. Also, the a_{eq} were lower, especially at higher speeds.

These results suggest that the LQ-Servo controller could be a promising option for real vehicle tests.

In future work, the integration of machine learning methods with classical controllers for lateral vehicle control will be considered. The robustness of these algorithms against parametric uncertainties, such as shifts in the center of mass, payload changes, and tire variations, will be evaluated. Additionally, their performance in handling lateral disturbances like side wind gusts will be analyzed, with a focus on both vehicle stability and passenger comfort, including the potential for motion sickness.

REFERENCES

AbdElmoniem, A., Osama, A., Abdelaziz, M., and Maged, S. A. (2020). A path-tracking algorithm using predictive stanley lateral controller. *International Journal of Advanced Robotic Systems*, 17(6):1729881420974852.

Athans, M. and Falb, P. L. (2013). *Optimal control: an introduction to the theory and its applications*. Courier Corporation.

Cascetta, E., Carteni, A., and Di Francesco, L. (2022). Do autonomous vehicles drive like humans? a turing approach and an application to sae automation level 2 cars. *Transportation research part C: emerging technologies*, 134:103499.

de Winkel, K. N., Irmak, T., Happee, R., and Shyrokau, B. (2023). Standards for passenger comfort in automated vehicles: Acceleration and jerk. *Applied Ergonomics*, 106:103881.

Gáspár, P., Szabó, Z., Bokor, J., and Németh, B. (2016). Robust control design for active driver assistance systems. *Springer, Book*, 10:978–3.

Jagelčák, J., Gnap, J., Kuba, O., Frnda, J., and Kostrzewski, M. (2022). Determination of turning radius and lateral acceleration of vehicle by gnss/ins sensor. *Sensors*, 22(6):2298.

Kilinc, A. S. and Baybura, T. (2012). Determination of minimum horizontal curve radius used in the design of transportation structures, depending on the limit value of comfort criterion lateral jerk. *TS06G-Engineering Surveying, Machine Control and Guidance*.

Li, D., Zhao, D., Zhang, Q., and Chen, Y. (2019). Reinforcement learning and deep learning based lateral control for autonomous driving [application notes]. *IEEE Computational Intelligence Magazine*, 14(2):83–98.

Luciani, S., Bonfitto, A., Amati, N., and Tonoli, A. (2020). Model predictive control for comfort optimization in assisted and driverless vehicles. *Advances in Mechanical Engineering*, 12(11):1687814020974532.

Mashadi, B., Mahmoudi-Kaleybar, M., Ahmadizadeh, P., and Oveisi, A. (2014). A path-following driver/vehicle model with optimized lateral dynamic controller. *Latin American journal of solids and structures*, 11:613–630.

Mathew, T. V. (2012). Genetic algorithm. *Report submitted at IIT Bombay*, 53.

Menhour, L., Lechner, D., and Charara, A. (2012). Design and experimental validation of linear and nonlinear vehicle steering control strategies. *Vehicle system dynamics*, 50(6):903–938.

Mesghali, K. (2021). Control tuning of autonomous vehicles considering performance-comfort trade-offs. Master's thesis, School of Industrial and Information Engineering.

Moreno-Gonzalez, M., Artuñedo, A., Villagra, J., Join, C., and Fliess, M. (2022). Speed-adaptive model-free lateral control for automated cars. *IFAC-PapersOnLine*, 55(34):84–89.

Németh, B. and Gáspár, P. (2011). Road inclinations in the design of LPV-based adaptive cruise control∗. *IFAC Proceedings Volumes*, 44(1):2202–2207.

Poussot-Vassal, C., Sename, O., Dugard, L., and Savaresi, S. (2011). Vehicle dynamic stability improvements through gain-scheduled steering and braking control. *Vehicle System Dynamics*, 49(10):1597–1621.

Rajamani, R. (2011). *Vehicle dynamics and control*. Springer Science & Business Media.

Samuel, M., Hussein, M., and Mohamad, M. B. (2016). A review of some pure-pursuit based path tracking techniques for control of autonomous vehicle. *International Journal of Computer Applications*, 135(1):35–38.

Sever, M., Zengin, N., Kirli, A., and Arslan, M. S. (2021). Carsickness-based design and development of a controller for autonomous vehicles to improve the comfort of occupants. *Proceedings of the Institution of Mechanical Engineers, Part D: Journal of Automobile Engineering*, 235(1):162–176.

Tagne, G., Talj, R., and Charara, A. (2015). Design and comparison of robust nonlinear controllers for the lateral dynamics of intelligent vehicles. *IEEE Transactions on Intelligent Transportation Systems*, 17(3):796–809.

Tóth, R. (2010). *Modeling and identification of linear parameter-varying systems*, volume 403. Springer.

Wang, L. (2009). *Model predictive control system design and implementation using MATLAB*, volume 3. Springer.

Zhang, Y., Sun, P., Yin, Y., Lin, L., and Wang, X. (2018). Human-like autonomous vehicle speed control by deep reinforcement learning with double q-learning. In *2018 IEEE intelligent vehicles symposium (IV)*, pages 1251–1256. IEEE.

Zhu, M., Wang, X., and Wang, Y. (2018). Human-like autonomous car-following model with deep reinforcement learning. *Transportation research part C: emerging technologies*, 97:348–368.

Zin, A., Sename, O., Gaspar, P., Dugard, L., and Bokor, J. (2008). Robust LPV-$\mathcal{H}\infty$ control for active suspensions with performance adaptation in view of global chassis control. *Vehicle System Dynamics*, 46(10):889–912.